A Microionizer for Portable Mass Spectrometers Using Double-Gated Isolated Vertically Aligned Carbon Nanofiber Arrays

Liang-Yu Chen, Luis Fernando Velásquez-García, *Senior Member, IEEE*, Xiazhi Wang, K. Teo, and Akintunde Ibitayo Akinwande, *Fellow, IEEE*

***Abstract*—We report a gas ionizer based on arrays of microfabricated double-gated isolated vertically aligned carbon nanofibers (VA-CNFs) for application in low-power portable mass spectrometers. Field-emitted electrons from VA-CNFs are accelerated to high energy and subsequently collide with neutral gas molecules, leading to ionization/fragmentation of the molecules. Double-gated field-emitter arrays with isolated VA-CNF tips were fabricated using a photoresist planarization technique. Two types of devices were fabricated and characterized. The first type of device has the emitter tip in the same plane as the extraction gate, and the second type of device has the emitter tip 900 nm below the extraction gate. All devices were made using a process that results in gate and focus diameters of 1.7 and 4.2 μm, respectively. When operated as a field-emitted electron impact ionizer (EII), for the same ion current, the ionization efficiency (ratio of ions to emitted electrons) increased from 0.005 to 0.05 as the pressure is increased between 5×10^{-6} and 1×10^{-3} torr. In comparison with EIIs based on thermionic electron sources, the power dissipation reduced from $>$ 1 W to 100 mW.**

***Index Terms*—Ionization, vacuum technology.**

I. Introduction

PORTABLE mass spectrometers (MSs) require low power and compact gas ionizers. State of the art instruments use electron impact ionizers (EIIs) based on thermionic emission sources [1]–[3], which produce electrons from a heated filament. Thermionic electron sources consume high power, typically $>$ 1 W, and are hence not suitable for portable low-power MSs. In addition, the EIIs based on thermionic electron sources have slow switch-on time and are not robust. These disadvantages could be eliminated if the thermionic electron source is replaced by a cold electron source such as a field-emission array (FEA). The advantage of using a field-emission electron source for electron impact ionization is that field emission occurs at room temperature and does not require heating. In the field-emission process, a voltage is applied between a sharp tip and a conducting gate with an annular aperture to create a large electric field at the tip apex. This applied electric field bends the vacuum level and thus narrows the energy barrier between electrons in the tip and the vacuum, leading to electron tunneling. Electrons are emitted as soon as the electric field is applied, and consequently, this process has a fast switch-on time. There are several other significant advantages of replacing thermionic electron sources with a field-emission-electron source in an EII [4]. These advantages include elimination of thermal cracking of delicate molecules, avoidance of outgassing due to the thermal load, and the most important is the significant reduction in pumping requirement due to the elimination of the hot filament.

While field emission-based electron impact ionizers have the above advantages, they are very vulnerable to tip erosion by back streaming ions because the tip is typically biased at a lower potential relative to the extraction gate and the accelerating electrode. To reduce the vulnerability to back ion tip erosion, a second gate positioned between the extraction gate and the accelerating anode and biased at lower voltage relative to the tip, focuses the field-emitted electrons and collects the back streaming ions, thus protecting the tip.

This paper presents the design, fabrication, and characterization of an EII based on a microfabricated double-gated vertically aligned carbon nanofiber (VA-CNF) FEAs. When voltages are applied to the extraction gate and focus, the double-gated VA-CNF arrays emit electrons. Ions are generated when the electron beam from the FEAs collides with neutral molecules after being accelerated to a high energy.

II. Device Structure and Model

The EII uses a double-gated field-emitter array as a cold electron source to reduce power dissipation. Electrons accelerated to high energy collide with neutral molecules to create ions that are fragments of the neutral molecules. The double-gated FEA has a second gate (focus gate) stacked above the first gate (extraction gate), as shown in Fig. 1. The emitter tip is a VA-CNF that is symmetrically placed between the two annular apertures in the extraction gate and focus gate electrodes. The

Manuscript received September 26, 2010; revised February 22, 2011 and April 4, 2011; accepted April 11, 2011. Date of current version June 22, 2011. This work was supported in part by the Defense Advanced Research Projects Agency Microsystems Technology Office and in part by the U.S. Army Soldier Systems Center under Contract W911QY-05-1-0002. The review of this paper was arranged by Editor A. M. Ionescu.

L.-Y. Chen was with the Massachusetts Institute of Technology, Cambridge, MA 02139 USA.

L. F. Velásquez-García is with the Microsystems Technology Laboratories, Massachusetts Institute of Technology, Cambridge, MA 02139 USA (e-mail: lfvelasq@mit.edu).

X. Wang is with the Massachusetts Institute of Technology, Cambridge, MA 02139 USA (e-mail: xw224@ mit.edu).

K. Teo was with the Cambridge University, Cambridge CB3 0FA, U.K.

A. I. Akinwande is with the Department of Electrical Engineering and Computer Science, Massachusetts Institute of Technology, Cambridge, MA 02139 USA (e-mail: akinwand@mtl.mit.edu).

Color versions of one or more of the figures in this paper are available online at http://ieeexplore.ieee.org.

Digital Object Identifier 10.1109/TED.2011.2145419

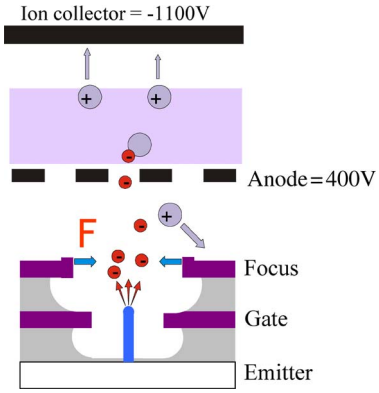

Fig. 1. Double-gated VA-CNF device operated as a field-emitted EII.

electrodes are both thin films of doped amorphous Si. Two silicon dioxide insulating films separate the emitter electrode from the extraction gate electrode and the focus electrode from the extraction gate electrode. The anode is a perforated screen, which accelerates the electrons to high energy, allowing a significant fraction of the emitted electrons to pass through to the collision/ionization region. The anode is biased at a relatively high positive voltage (> the extraction gate bias). The collector is also perforated to allow ions to exit the ionizer, and it is biased at lower voltage than the anode in order to set up a field that will allow the extraction of the ions. When appropriate voltages are applied to the extraction and focus electrodes, an enhanced electrostatic field is created at the VA-CNF tip, which leads to the extraction of electrons. The extracted electrons are accelerated by the anode toward the ionization region where the electrons collide with neutral molecules, resulting in ionization. The second gate (focus), which is typically biased at a lower potential than the extraction gate, serves two purposes. One function of the focus is to collimate/focus the extracted electrons. The second function of the focus is to attract and absorb back streaming ions, which reduces the chances of ions bombarding the tip.

A. *Field-Emission-Electron Source*

The double-gated VA-CNF array is the field-emission-electron source for the ionizer. It has four terminals—emitter, extraction gate, focus and anode. It can be operated as a four-terminal device in which the focus and the extraction gate are biased at different voltages, or it can be operated as a three-terminal device in which case the focus and extraction gate are biased at the same voltage.

Field-Emission Model: The emission current depends on electrostatic field F at the tip surface, which is a function of the bias voltages applied to both gates. Thus, the emission current depends on both the extraction gate bias voltage V_G and the focus bias voltage V_F. The field F at the tip surface is related to V_G and V_F through the gate field factor β_G and the focus field factor β_F, respectively. Using superposition, the tip apex field is expressed as $F = \beta_G V_G + \beta_F V_F$. The Fowler–Nordheim (FN) equation is used to calculate the total field-emission current. The FN equation approximates the electron transmission probability using the Wentzel–Kramers–Brillouim formulation [5], [6]. Assuming the effective emitting area is α, then the emission current for the double-gate FEA (four-terminal FEA) is given by

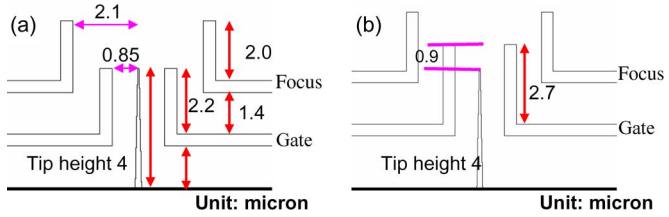

Fig. 2. Schematic of the two completed devices with dimension details (a) Device with the tip in-plane with the gate and (b) device with the tip 900 nm below the gate.

$$I(V_G, V_F) = \frac{\alpha \times A}{1.1 \times \phi} \times \exp\left[\frac{B \times 1.44 \times 10^{-7}}{\sqrt{\phi}}\right] \times (\beta_G V_G + \beta_F V_F)^2 \times \exp\left[-\frac{0.95 \times B \times \phi^{3/2}}{\beta_G V_G + \beta_F V_F}\right] \quad (1)$$

where $A = 1.56 \times 10^{-6}$, $B = 6.87 \times 10^7$, and ϕ is the work-function of the tip material.

When the double-gated FEA is characterized as a three-terminal FEA, the focus and the gate are biased at the same voltages, i.e., $V_G = V_F$. In this situation, the tip apex field can be expressed as

$$\beta_{\text{eff}} V_G = \beta_G V_G + \beta_F V_F = (\beta_G + \beta_F) V_G \quad (2)$$

and the field factor β_{eff} can be express as

$$\beta_{\text{eff}} = \beta_G + \beta_F. \quad (3)$$

Hence, the emission current for the three-terminal FEA is given by

$$I(V_G) = \frac{\alpha \times A}{1.1 \times \phi} \times \exp\left[\frac{B \times 1.44 \times 10^{-7}}{\sqrt{\phi}}\right] \times (\beta_{\text{eff}} V_G)^2 \times \exp\left[-\frac{0.95 \times B \times \phi^{3/2}}{\beta_{\text{eff}} V_G}\right]. \quad (4)$$

Field Factors: To estimate the value of the gate field factor β_G, focus field factor β_F, and effective field factor β_{eff} (when $V_F = V_G$), two models with the dimensions specified in Fig. 2(a) and (b), respectively, were built in MATLAB using the finite-element method. Both models have gate aperture radius of 0.85-μm and focus apertures of 2.1-μm, which corresponds to the apertures that we later experimentally obtained. One of the models has the tip aligned to the plane of the gate aperture, and the other model has the tip 900 nm below the gate aperture, which again corresponds to what we later experimentally obtained. In this paper, nickel is used as the catalyst material to grow isolated vertically aligned CNFs, and the Ni disks have a thickness of 4 nm and a diameter of 250 nm. A disk with these dimensions has a volume of 1.96×10^{-16} cm^3, which, theoretically, would form a sphere with a radius of 36 nm during the anneal that occurs during VA-CNF growth. Thus, the tip radius was assumed to be 36 nm for the MATLAB simulation. The purpose of the MATLAB models is to determine how the potential applied to the two

gates affect the electric field generated at the tip when the relative positions of the tip and the gate are different. From these two models, we obtained $\beta_G = 1.19 \times 10^6$ [V/cm], $\beta_F = 3.07 \times 10^5$ [V/cm], and the ratio of the field factors β_F/β_G is 0.272 when the tip is in-plane with the gate. When the tip is 900 nm below the gate, $\beta_G = 4.97 \times 10^5$ [V/cm], $\beta_F = 1.12 \times 10^4$ [V/cm], and the ratio of the field factors β_F/β_G is 0.023, indicating considerable screening of the tip from the influence of the focus gate by the extraction gate.

Using the same models, β_{eff} as a function of the tip radius in the double-gated structure can be deduced. When the tip is in-plane with the extraction gate and $V_F = V_G$

$$\beta_{\text{eff}} = \frac{11.2 \times 10^6}{r^{0.848}} \text{ [V/cm]}.$$

When the tip is 900 nm below the extraction gate and $V_F = V_G$

$$\beta_{\text{eff}} = \frac{47.5 \times 10^5}{r^{0.848}} \text{ [V/cm]}$$

where r is in nanometers. These two relationships are similar but not exactly the same due to the different tip positions relative to the extraction gate [6].

B. EII Model

In electron impact ionization, electrons are first extracted from the field-emitter tips and then accelerated to an energy several times higher than the gas molecules' ionization energies. The ionization efficiency $(I_I(E)/I_E(E))$ is given by [7]

$$\frac{I_I(E)}{I_E(E)} = \rho \times L \times \sigma_{\text{Total}}(E). \tag{5}$$

In the equation, ρ is density of neutral molecules in the gas, L is the collision path length, and $\sigma(E)$ is the total ionization cross section. Usually, for most gas molecules, the peak of the ionization cross section is of the order of 10^{-16}cm^2.

In this paper, the electron beam was generated by field emission, and the electron emission current can be calculated from the FN equation [5], [6]. Using (5), the ion current is estimated from the number density of molecules in the gas ρ, the collision path length L, the total ionization cross section $\sigma(E)$, and the electron current (I_E).

III. Ionizer Fabrication

The VA-CNF arrays were designed such that the electric field generated at the tip is maximized, and the shielding effect from the neighbors is minimized. Furthermore, the device is capable of handling high voltages. The fabrication of the double-gated CNF structure starts with the definition of a 250-nm diameter and 4-nm-thick Ni catalyst at each emission site with 10-μm pitch by E-beam lithography and liftoff technique [10]. The catalyst size guarantees nucleation of a single Ni dot at each site [10], [11] and subsequent growth of an isolated 4-μm-tall VA-CNF using plasma-enhanced chemical vapor deposition (PECVD) at 725 °C, as shown in Fig. 3.

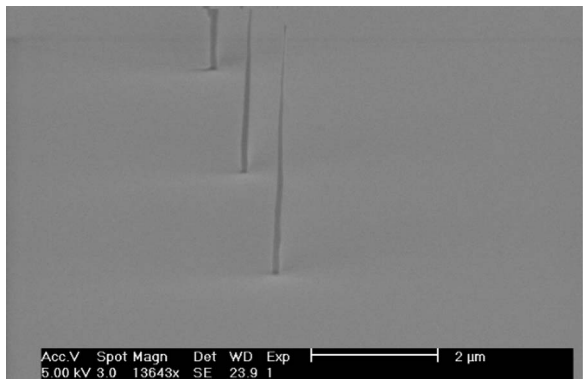

Fig. 3. Single VA-CNFs of 4 μm tall using PECVD.

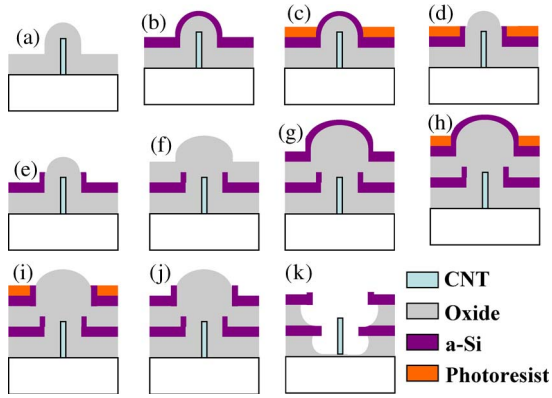

Fig. 4. Schematic of the double-gated VA-CNF device fabrication process.

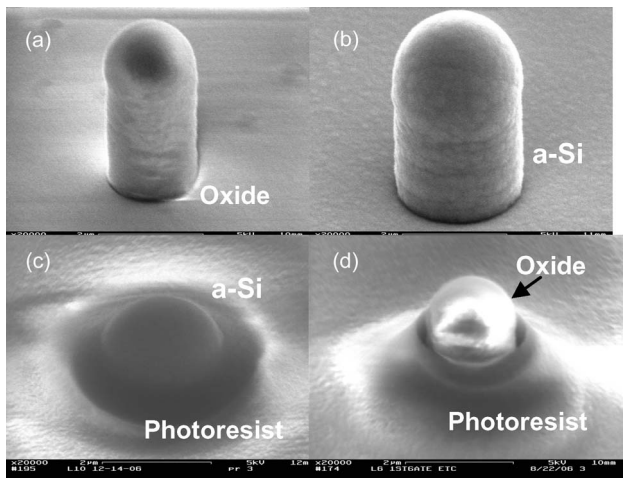

Fig. 5. SEMs of (a) a VA-CNF covered by 1.4-μm oxide, (b) a 0.4-μm conformal layer of doped a-Si on top of the oxide, (c) a layer of PR spun at a high speed, and (d) a-Si was removed to define the gate.

Once CNF was grown, the extraction gate and the out-of-plane focus gate were fabricated with a novel photoresist (PR) planarization technique, and the fabrication process flow is shown in Fig. 4. This fabrication process starts with the formation of the gate insulator and the gate electrode (steps A–E). A conformal layer of PECVD oxide was deposited as the gate insulator to separate CNFs and the gate material (amorphous-Si), as shown in Fig. 5(a). Next, a conformal PECVD-doped a-Si was deposited on top of the oxide to form a gate electrode [see Fig. 5(b)]. Steps C–E illustrate the self-aligned technique. The

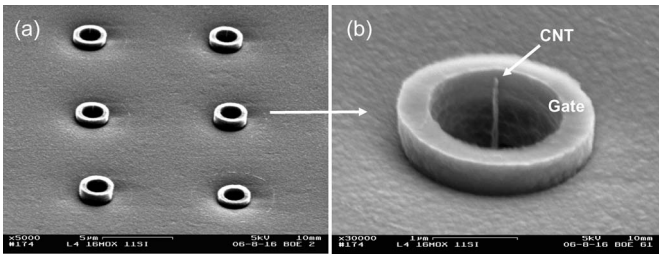

Fig. 6. SEM pictures of (a) an array of single-gated CNF FEA and (b) an individual single-gated CNF device.

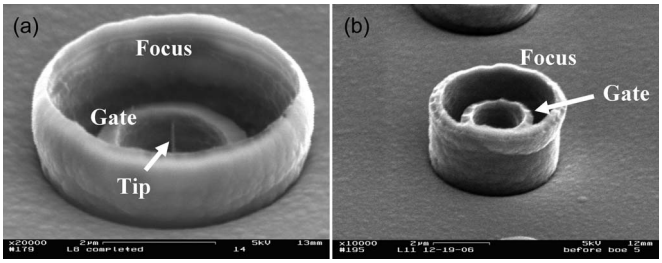

Fig. 7. Side views of the two double-gated isolated VA-CNF devices. (a) When the tip is in-plane with the gate and (b) when the tip is 900 nm below the gate.

PR was spun on the wafer at a high speed, which resulted in PR surface planarization, without using chemical mechanical polishing (CMP) [see Fig. 5(c)]. This smooth PR layer defined the structure of the gate aperture. An anisotropic silicon reactive-ion etching (RIE) was then used to etch the a-Si [see Fig. 5(d)] and thus open the gate aperture. By varying the etch time, we can change the tip position with respect to the extraction gate. With less etch time, less a-Si is removed, and the tip ends up below the extraction gate. In this paper, two structures were made, one has the tip in-plane with the gate and the other has the tip 900 nm below the gate. After the gate aperture was patterned by RIE, the PR was then removed. Fig. 6 shows scanning electron microscope (SEM) pictures of an array of a single-gated CNF structure using this technique. The fabrication of the double-gated VA-CNF field-emitter array continues with the formation of the focus insulator and the focus electrode (steps F–J) by repeating the steps A–E. The last step of the fabrication process is to expose the CNF by removing the oxide between the focus electrode, gate electrode, and the CNF field emitter using buffered oxide etch (step K). The side views of the two complete double-gated CNF devices for the tip is in-plane with the gate and the tip is 900 nm below the gate are shown in Fig. 7(a) and (b), respectively. This technique offers a very fast, fairly uniform, and well-controlled planarization method of making the self-aligned gates, which replaces the CMP technique that has been reported in [12]–[14]. In this paper, a 32×32 CNF array is characterized in both field emission and EII experiments.

IV. Field Emission Characterization

A. Three-Terminal Field-Emission Characterization

The double-gated CNF arrays were first characterized as three-terminal field emitters with the gate and focus biased at the same voltages. To ensure the field-emission data is reproducible, a series of 12 I–V sweeps, which consisted of a series current–voltage measurements as the extraction gate voltage is stepped up, immediately followed by a series of current–voltage measurements as the extraction gate voltage is stepped down, were performed in sequence. Anode current versus extraction gate voltage plots are shown in Fig. 8(a) for the device with tips that are in-plane with the gate and in Fig. 8(b) for the device with tips that are 900 nm below the gate. Note that there is a nonzero current of 1×10^{-11} A, even at 0 V. This is the noise floor of the experimental setup, confirmed by a blank test without any wafer.

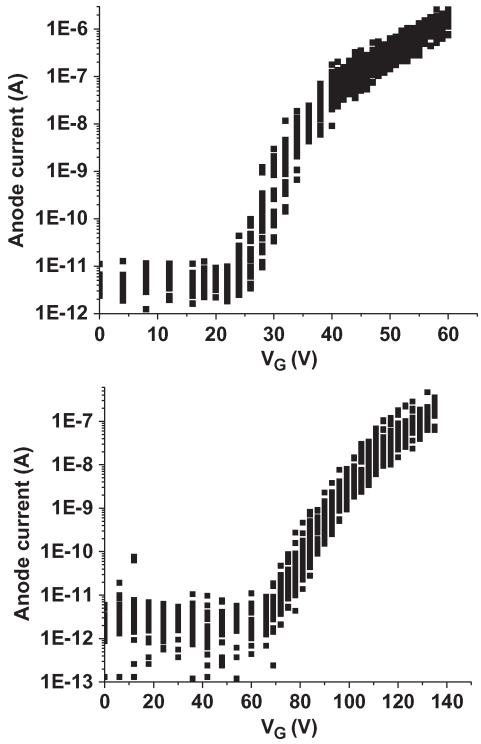

Fig. 8. Anode current I_A versus gate voltage V_G showing repeatable field emission. (a) When the tip is in-plane with the gate and (b) when the tip is 900 nm below the gate.

Rewriting (4) as

$$I = a_{\mathrm{FN}} V_G^2 \exp\left(\frac{-b_{\mathrm{FN}}}{V_G}\right) \tag{6}$$

with

$$a_{\mathrm{FN}} = \frac{\alpha A \beta_{\mathrm{eff}}^2}{1.1\phi} \exp\left[\frac{B(1.44 \times 10^{-7})}{\phi^{1/2}}\right] \tag{7}$$

$$b_{\mathrm{FN}} = \frac{0.95 B \phi^{3/2}}{\beta_{\mathrm{eff}}} \tag{8}$$

we can extract the FN parameters a_{FN} and b_{FN} from a plot of $\mathrm{Ln}(I_A/V_G^2)$ versus $1/V_G$. Fig. 9(a) and (b) are the FN plots of the data shown in Fig. 8(a) and (b) respectively (a_{FN} is the intercept, and b_{FN} is the slope of the FN plot) with the error and standard deviation (SD) of the least-square fit. From the FN plot, we observe that the values of R are close to -1, and that the SD is small.

Once the b_{FN} and a_{FN} values were extracted, (7) and (8) were used to calculate the effective field factor β_{eff} and

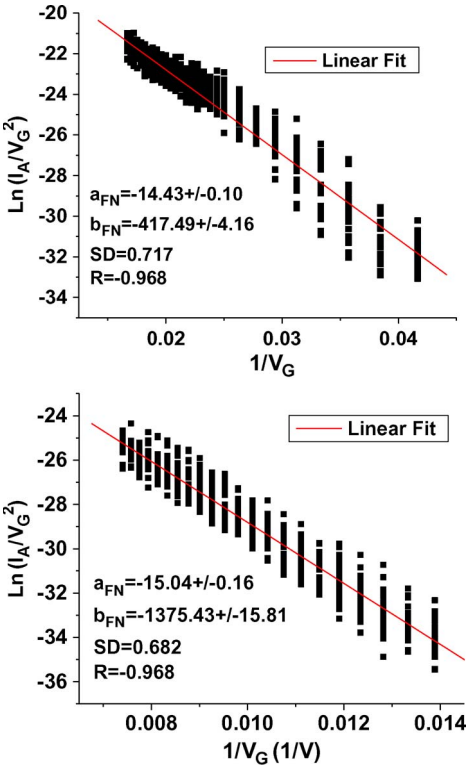

Fig. 9. FN analysis of the field emission data shown in Fig. 8. (a) When the tip is in-plane with the gate and (b) when the tip is 900 nm below the gate.

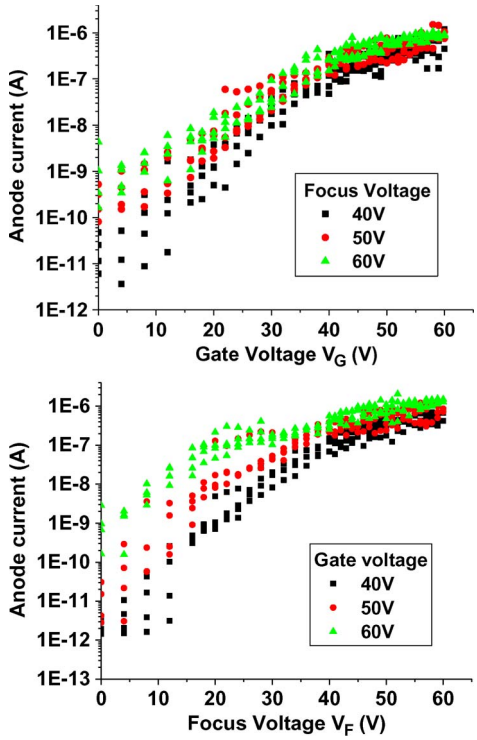

Fig. 10. Four-terminal I–V data for the device with the tip in-plane with the gate. (a) The gate transfer characteristic (I_A versus I_G at fixed V_F). (b) The focus transfer characteristic (I_A versus I_F at a fixed V_G).

the effective emitting area α. Assuming the workfunction of CNF is 5 eV, we obtained $\beta_{\text{eff}}, = 1.75 \times 10^6$ [V/cm] and $\alpha = 75.79$ [nm^2] for the device with tip is in-plane with the gate and $\beta_{\text{eff}}, = 5.31 \times 10^5$ [V/cm] and $\alpha = 446.95$ [nm^2] for tip is 900 nm below the gate. Using the MATLAB models described earlier, the estimated tip radius is about 3.2 nm for the device with a tip that is in-plane with the gate and 13.2 nm for device with tip that is 900 nm below the gate. This tip radius is less than the catalyst sphere that formed from the catalyst disks that used to grow the CNFs. There are several reasons why the radii of the CNFs are in reality smaller than 36 nm. The Ni disks were annealed at a high temperature to form Ni catalysts, prior to growth of the CNFs. During this process, silicon substrate could have reacted with Ni to form nickel silicide, resulting in loss of Ni. Another possible explanation is that Ni was lost during the CNT growth process. Merkulov *et al.* attribute the loss of catalysts to two main mechanisms [15]. One is, during the growth, the ion sputtering and/or dispersion of the catalyst material within the CNF reduces the size of the nanoparticle. The other is, as the size of the catalyst decreases, the upper part of CNF becomes thinner and eventually breaks off from the tip during the growth. For the tip that is in-plane with the gate structure, the estimated tip radius of 3.2 nm is much smaller than the estimated tip radius of 13.2 nm for the tip that is 900 nm below the gate structure. This suggests that there are tips that are much smaller than the average tip radius, and these tips with smaller radius dominate. This is consistent with earlier literature reports [16], [17] which reported a distribution of the Si tip radii and that the smaller tip radii dominate electron emission from the tips. This is explained by the exponential dependence of field-emission current on the tip radius.

B. Four-Terminal Field-Emission Characterization and Discussion

To characterize the array as a four-terminal device, the extraction gate and the focus gate were biased at different voltages. As indicated earlier, the tip electric field depends on both extraction gate and the focus gate for the double-gated FEA. To investigate the influence of the extraction gate and the focus gate on the emission current, the gate field factor β_G and the focus field factor β_F need to be extracted from the I–V data. To accomplish this goal, two transfer characteristics were obtained. One is the focus transfer characteristics, which shows the variation of the anode current as a function of the focus voltage with the gate voltage fixed. The other is the gate transfer characteristics, which shows the variation of the anode current as a function of the gate voltage with the focus voltage fixed. The two transfer characteristics of the tip that is in-plane with the gate are shown in Fig. 10 and of the tip is 900 nm below are shown in Fig. 11.

To extract the gate field factor β_G and the focus field factor β_F, anode current I_A, gate current I_G, and focus current (IF) are added together to compute the total emission current. We fit the emission current to (1) using Origin Pro7 software package [18]. There are several uncertainties that we need to consider. The value of the tip workfunction ϕ randomly fluctuates with time, and the effective emitting area α is only an estimate that we obtained from the three-terminal measurements. Thus, Dvorson suggested that instead of focusing on studying β_G and β_F, the ratio of the field factors β_F/β_G is more stable and serves as a reliable estimate [19]. Figs. 12 and 13 show the fit of the data for the device that has the tip in-plane

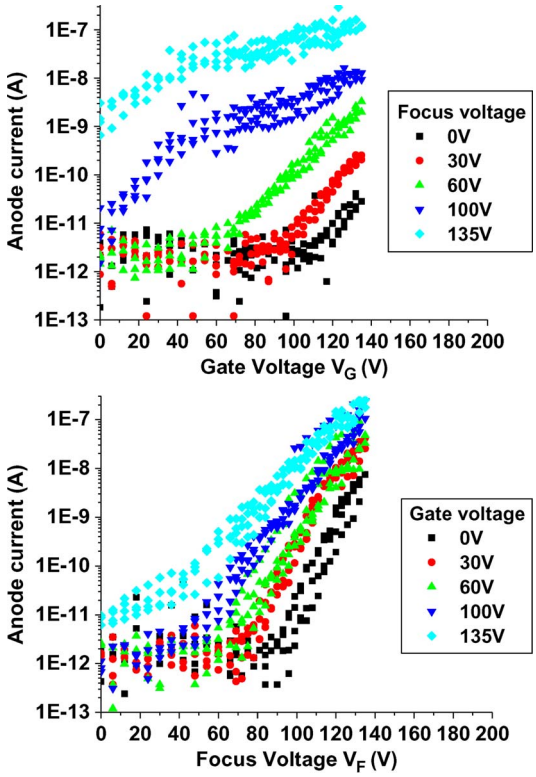

Fig. 11. Four-terminal I–V data for the device with the tip 900 nm below the gate. (a) The gate transfer characteristic (I_A versus I_G at fixed V_F). (b) The focus transfer characteristic (I_A versus I_F at a fixed V_G).

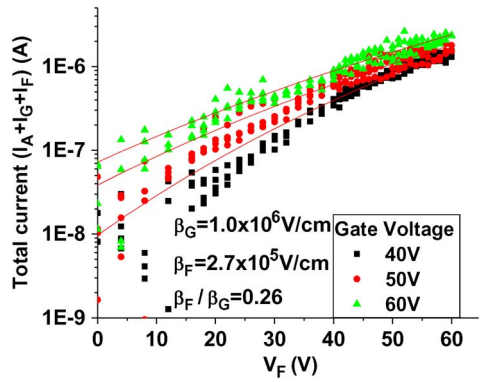

Fig. 12. Device with the tip in-plane with the gate: Total emission current versus focus voltage at fixed gate voltages. β_F and β_G are extracted based on (1).

with the gate and the device that has the tip is 900 nm below the gate, respectively. The same two MATLAB models described earlier are used to estimate β_G and β_F. Table I summarizes these parameter estimates.

From the fit of the four-terminal I–V data, summarized in Table I, the ratio of β_F/β_G for the device with tip in-plane with the gate is 0.26, compared with 0.02 for the device with the tip at 900 nm below the gate. The values of β_F and β_G and the ratios of β_F/β_G calculated from the MATLAB simulation for both devices are consistent with the experimental data. This result agrees with the SEMs shown in Fig. 7 and are consistent with the results in [12], [14], and [19].

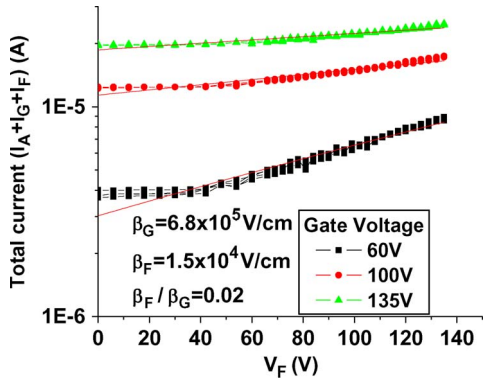

Fig. 13. Device with the tip 900 nm below the gate: Total emission current versus focus voltage at fixed gate voltages. The β_F and β_G are extracted based on (1).

TABLE I
SUMMARY OF β_F, β_G, AND THE RATIO OF β_F/β_G FROM THE FOUR-TERMINAL DATA AND THE MATLAB SIMULATIONS

	4-TERMINAL DATA			Matlab Simulation		
	β_F [V/cm]	β_G [V/cm]	β_F/β_G	β_F [V/cm]	β_G [V/cm]	β_F/β_G
Tip 900nm below the gate	1.51x10^4	6.8x10^5	0.02	1.12x10^4	4.97x10^5	0.02
Tip in-plane with gate	2.71x10^5	1.01x10^6	0.26	3.07x10^5	1.19x10^6	0.26

V. ELECTRON IMPACT IONIZATION CHARACTERIZATION

In the EII experiment, the double-gated FEA was biased as a three-terminal device $V_G = V_F$, whereas the emitters were biased at 0 V. A perforated screen anode is placed right above the device ($L = 0.5$ cm) and is biased at a higher voltage (400 V) than the gate voltage to accelerate electrons before impacting with gas molecules. The electron pass-through rate is 85%. This is measured by applying a same voltage on the ion collector and comparing the current from the ion collector and the anode gate. Then, the collector voltage is set at -1100 V to collect the ions generated by EII and repel electrons. The gas used in these sets of experiments is argon.

A. Electron Current Versus Ion Current at a Fixed Pressure

In the EII process, electrons are first extracted from the field-emitter tip and then accelerated up to an energy several times higher than the gas molecules' ionization energy. Ionization takes place when these energetic electrons collide with gas molecules. As shown in (5), the ion current depends on the number of electrons and the density of the gas molecules in the chamber at fixed L and $\sigma(E)$. Here, we demonstrate this linear relationship by varying the electron current and the chamber pressure, which is measured by a MKS 431 cold cathode vacuum sensor.

To precisely control the chamber pressure, argon (Ar) is passed into the chamber by a needle valve, which can precisely restrain the amount of Ar flowing into the chamber. The ion

current I_I and the electron current I_E are monitored and recorded while varying the extraction gate voltage ($V_F = V_G$). This experiment was run at different pressures: 5×10^{-7} torr, 5×10^{-6} torr, 5×10^{-5} torr, and 5×10^{-4} torr. The I–V characteristics of EII at the different pressures are plotted in Fig. 14(a)–(d), respectively.

Electron currents and the molecular density (calculated as $P/K.T$, where P is the gas pressure, K is Boltzmann's constant and T is the gas temperature) are plugged into (5). L is 0.5 cm, which is the distance between the ion collector and the screen anode. The screen anode is biased at 400 V, which gives us the ionization cross section of 1.5×10^{-16} cm^2 for Ar+ [8]. Using these parameters, the predicted ion currents are plotted with measured ion currents in Fig. 14. As the pressure increases, the ion currents increase with electron currents.

B. Pressure Dependence

In Fig. 14, we observe that as pressure increases, ion current increases. Furthermore, to verify the linear relationship between pressure and the ion current, ion currents (collector current) and electron current (screen/anode current) were measured at different pressures from 5×10^{-6} to 1×10^{-3} torr. As shown in Fig. 15, the linear relationship holds between pressure and the ratio of the ion current to the electron current. Both correlation coefficient (R) values of these two devices are very close to $+1$, indicating that the pressure and the ratio of the ion current to electron current are highly correlated. The SD shows that all the data tightly gathered. From the linear relationship between pressure and the ratio of ion current and electron current, the ionization cross section can be estimated. Using (5), and knowing electron current, pressure, and L, the ionization cross section is estimated to be 1.2×10^{-16} cm^2, which is fairly closed to the value we obtained from the literature (1.5×10^{-16} cm^2) [8].

VI. Discussion

The turn-on voltage of the double-gated VA-CNF field-emitter array presented in this paper is comparable to values reported in [6], [12], [19], and [14]. This is consistent with the values of the gate and focus field factors extracted from the data and the tip radii obtained from SEM metrology. The CNFs are expected to have a tip radius distribution [10], resulting in a distribution of the field factors [20], which implies that the turn on of the device will be dominated by the smallest tip radii. This in part explains why the tip radii extracted from the I–V characteristics and the FN analysis seem to be much smaller than the radii that has been obtained from the SEM or projected from the analysis of catalyst size.

Our four-terminal I–V characterization of the double-gate VA-CNF field-emitter array suggest that the ratio of the focus field factor to the gate field factor (F/G) is an excellent indicator of the relative position of the CNF relative to the extraction gate and the focus gate. From the fits of the experimental data, the extracted values of the focus (F) and gate (G) field factors clearly show that when the CNF tip is in the same plane as the extraction gate electrode, the ratio of the focus field factor to the gate field factor (F/G) is 0.26. This is consistent with geometric arguments that both the gate and the focus have a direct line-of-sight view of the emitter tip with the gate being closer and hence having a higher field factor. However, the gate field factor is not significantly higher, and F/G would be of the order 0.1–0.5. Using exact geometric dimensions of the double-gated VA-CNF field-emitter structure, simulations show

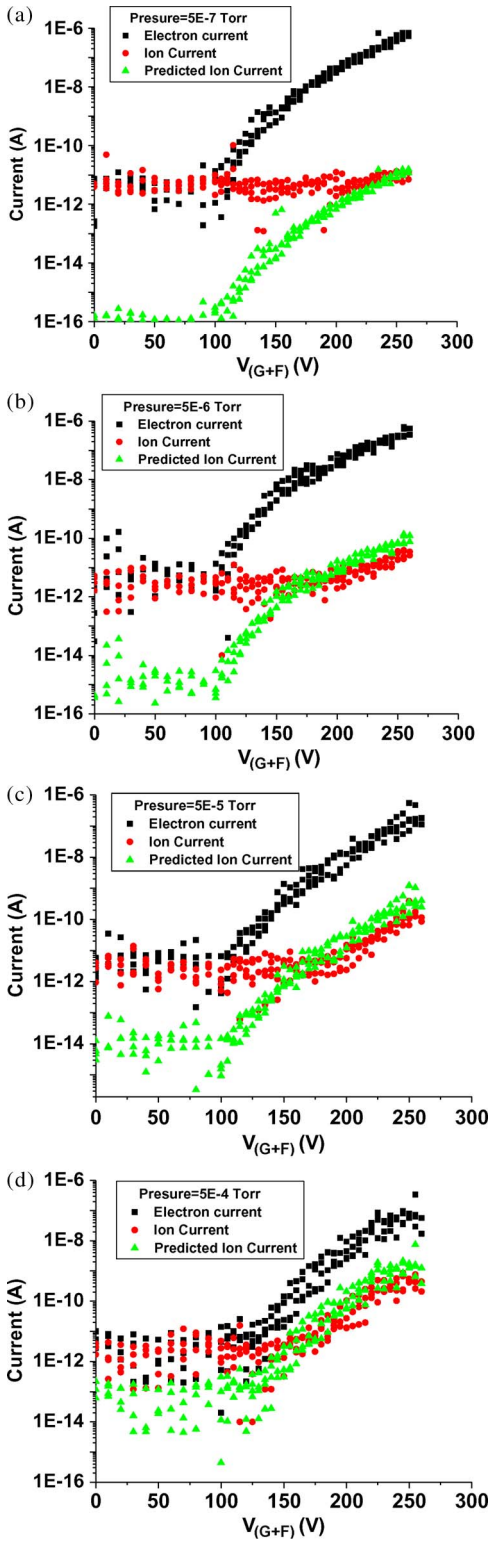

Fig. 14. Electron impact ionization data from the double-gated CNF FEA with the tips in-plane with the gate. (a) Pressure at 5×10^{-7} torr. (b) Pressure at 5×10^{-6} torr. (c) Pressure at 5×10^{-5} torr. (d) Pressure at 5×10^{-4} torr.

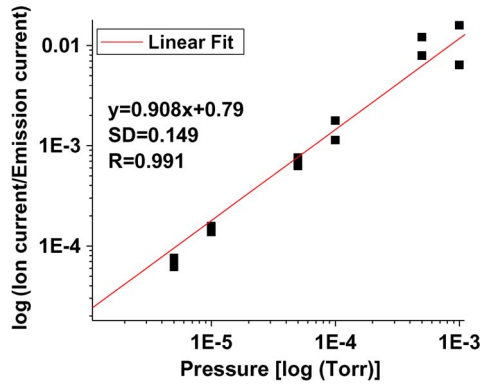

Fig. 15. Device with the tip in-plane with the gate: linear relationship between normalized ion current (I_I/I_S) versus pressure for the device with the tips in-plane with the gate. There is a linear relationship between the normalized ion current and the pressure.

that F/G is 0.26. On the other hand, when the tip is below the gate and there is no longer a direct line-of-sight view of the tip from the focus (meaning that the tip is screened by the gate), using the same geometric arguments, one would expect the ratio of the field factors to be much smaller than 0.1. Simulations using the exact geometric dimensions show that F/G is 0.02, which is consistent with the fact that the focus is screened by the gate. The value of F/G extracted from the experimental data is 0.02, which is consistent with both the geometric arguments and the simulations. Neo *et al.* has recently reported double-gated FEAs, which use a volcano structure in which the focus electrode is placed ≈500 nm below the tip and the extraction gate completely shielded the tip from the influence of the focus electrode [21]. While they did not specifically calculate F and G, the focus transfer characteristics of their device showed that the emission and anode currents are only weakly dependent on focus voltage. Their results suggested that F is very small and F/G is also very small, i.e., < 0.01. The values of F/G and the dependence on the position of the tip relative to the planes of the gate and focus electrodes are consistent with earlier works by Dvorson *et al.* [6], [12], [19], Chen and Akinwande [14], Itoh *et al.* [22], Yamaoka *et al.* [23], and Hosono *et al.* [24]. Neo *et al.* further examined double-gated volcano field-emitter arrays and their focusing properties in more detail [25]. From the focus transfer characteristics of these devices, the focus practically has no effect on the anode current or the emission current when the focus is fully shielded by the gate from the influence of the focus. In the other structures, there was a greater dependence of anode and emission current on the focus voltage. This is confirmed by the total emission current obtained from the three structures when the focus voltage V_F is 60 and 5 V.

The linear dependence of the ratio of the ion current to the electron current (I_I/I_E) when the double-gated VA-CNF field-emitter array is used as an electron source for the impact ionizer suggest that there is a single dominant impact ionization cross section and that the gas molecules are singly ionized. For the study of the pressure dependence of the ionizer, the focus and gate voltages were both kept at 250 V, whereas the anode/screen was biased at 400 V. Thus, the energy of the electron is slightly outside the region of maximum impact ionization cross section [8]. Bower *et al.* demonstrated an EII based on CNT field-emission-electron source [26]. Their device is based on a CNT forest as the emitter and a suspended and perforated MEMS structure as grid. The device was generally operated at higher pressures than the current device, the ion current are generally comparable for Ar. At a pressure of 1 mtorr, the current device demonstrated an ion-current/emission-current ratio of 10 : 2, whereas the device reported by Bower *et al.* demonstrated a corresponding ion-current/emission-current ratio of 10:4. The difference in current ratio could perhaps be explained by their device structure, which is not self-aligned, leading to excess grid interception. In a later work by Natarajan *et al.*, the device performance improved by an order of magnitude by using a four-electrode structure. The improved performance was attributed to an increase in the electron current contributing to ionization and improved ion collection efficiency [27]. At a pressure of 1 mtorr, the ion-current/emission-current ratio improved to 10 : 3. These results are in general agreement with the recent works on Bayard–Alpert vacuum gauges based of field-emitted electron sources [28]–[31]. The vacuum gauges determine pressure by measuring current resulting from electron impact ionization. The ionization gauges are able to obtain higher ion currents per field-emitted current by increasing the ionization path length and ion collection efficiency though the device construction.

VII. Conclusion

Double-gated field-emitter arrays with isolated VA-CNF tips have been fabricated using a PR planarization technique. Two types of devices have been fabricated. The first type of device has the emitter tip in the same plane as the extraction gate and the second type of device has the emitter tip 900 nm below the extraction gate. All the devices were made using a process that results in gate and focus diameters of 1.7 and 4.2 μm, respectively. The devices were first characterized as field emitters. From the three-terminal I–V characteristics, the tip radii were extracted using the MATLAB models. The four-terminal I–V characteristics yielded gate and focus transfer characteristics of the double-gated VA-CNF field-emitter arrays. The devices showed different characteristics due to the relative positions of the tip, with respect to the extraction gate. Total emission currents for both devices were computed and applied in the generalized FN equation to extract the values of gate and focus field factors. Electron impact ionization characterization of Ar was conducted using the double-gated VA-CNF as the electron source. The results show that the ion current linearly varies with electron current at a fixed pressure and that there is a linear relationship between the ratio of the ion current and the electron current and pressure, as expected from the electron impact ionization model.

Acknowledgment

The authors would like to thank the staff of Microsystems Technology Laboratories and the staff of NanoStructures Laboratory at Massachusetts Institute of Technology for the help during device fabrication. The vertically aligned carbon nanofiber were grown at Cambridge University Engineering Department fabrication facility.

REFERENCES

[1] E. de Hoffmann and V. Stroobant, *Mass Spectrometry: Principles and Applications*. Chichester, U.K.: Wiley, 2002.

[2] J. H. Gross, *Mass Spectrometry: A Textbook*. Berlin, Germany: Springer-Verlag, 2004.

[3] H. D. Beckey, *Principles of Field Ionization and Field Desorption Mass Spectrometry*. London, U.K.: Pergamon, 1977.

[4] T. E. Felter, "Cold cathode field emitter array on a quadrupole mass spectrometer: Route to miniaturization," *J. Vac. Sci. Technol. B, Microelectron. Nanometer Struct.*, vol. 17, no. 5, pp. 1993–1996, Sep. 1999.

[5] C. A. Spindt, I. Brodie, L. Humphrey, and E. R. Westerberg, "Physical properties of thin-film field emission cathodes with molybdenum cones," *J. Appl. Phys.*, vol. 47, no. 12, pp. 5248–5263, Dec. 1976.

[6] L. Dvorson, G. Sha, I. Kymissis, C.-Y. Hong, and A. I. Akinwande, "Electrical and optical characterization of field emitter tips with integrated vertically stacked focus," *IEEE Trans. Electron Devices*, vol. 50, no. 12, pp. 2548–2558, Dec. 2003.

[7] R. K. Asundi, "Electron path length in collision experiments," *Proc. Phys. Soc.*, vol. 82, no. 3, pp. 372–374, Sep. 1963.

[8] R. Rejoub, B. G. Lindsay, and R. F. Stebbings, "Determination of the absolute partial and total cross sections for electron-impact ionization of the rare gases," *Phys. Rev. A, Gen. Phys.*, vol. 65, no. 4, pp. 042713-1–042713-8, Apr. 2002.

[9] A. V. Kosarim, B. M. Smirnov, M. Capitelli, R. Celiberto, G. Petrella, and A. Laricchiuta, "Ionization of excited nitrogen molecules by electron impact," *Chem. Phys. Lett.*, vol. 414, no. 1–3, pp. 215–221, Oct. 2005.

[10] M. Chhowalla, K. B. K. Teo, C. Ducati, N. L. Rupesinghe, G. A. J. Amaratunga, A. C. Ferrari, D. Roy, J. Robertson, and W. I. Milne, "Growth process conditions of vertically aligned carbon nanotubes using plasma enhanced chemical vapor deposition," *J. Appl. Phys.*, vol. 90, no. 10, pp. 5308–5317, Nov. 15, 2001.

[11] K. B. K. Teo, S.-B. Lee, M. Chhowalla, V. Semet, T. B. Vu, O. Groening, M. Castignolles, A. Loiseau, G. Pirio, P. Legagneux, D. Pribat, D. G. Hasko, H. Ahmed, G. A. J. Amaratunga, and W. I. Milne, "Plasma enhanced chemical vapour deposition carbon nanotubes/nanofibres—how uniform do they grow?" *Nanotechnology*, vol. 14, no. 2, pp. 204–211, Feb. 2003.

[12] L. Dvorson, I. Kymissis, and A. I. Akinwande, "Double-gated silicon field emitters," *J. Vac. Sci. Technol. B, Microelectron. Nanometer Struct.*, vol. 21, no. 1, pp. 486–494, Jan. 2003.

[13] M. A. Guillorn, X. Yang, A. V. Melechkov, D. K. Hensley, M. D. Hale, V. I. Merkulov, and M. L. Simpson, "Vertically aligned carbon nanofiber-based field emission electron sources with an integrated focusing electrode," *J. Vac. Sci. Technol. B, Microelectron. Nanometer Struct.*, vol. 22, no. 1, pp. 35–39, Jan. 2003.

[14] L.-Y. Chen and A. I. Akinwande, "Aperture-collimated double-gated silicon field emitter arrays," *IEEE Trans. Electron Devices*, vol. 54, no. 3, pp. 601–608, Mar. 2005.

[15] V. I. Merkulov, A. V. Melechhko, M. A. Guillorn, D. H. Lowndes, and M. L. Simpson, "Sharpening of carbon nanocone tips during plasma-enhanced chemical vapor growth," *Chem. Phys. Lett.*, vol. 350, no. 5/6, pp. 381–385, Dec. 2001.

[16] D. G. Pflug, M. Schattenburg, H. I. Smith, and A. I. Akinwande, "Field emitter arrays for low voltage applications with sub 100 nm apertures and 200 nm period," in *IEDM Tech. Dig.*, 2001, pp. 179–182.

[17] M. Ding, G. Sha, and A. I. Akinwande, "Silicon field emission arrays with atomically sharp tips: Turn-on voltage and the effect of tip radius distribution," *IEEE Trans. Electron Devices*, vol. 49, no. 12, pp. 2333–2342, Dec. 2002.

[18] *Origin Pro7 Software Package Obtained Form OriginLab*. [Online]. Available: www.origin.lab.com

[19] L. Dvorson, "Micromachining and modeling of focused field emitters for flat panel displays," Ph.D. dissertation, Dept. Elect. Eng. Comput. Sci., MIT, Cambridge, MA, 2001.

[20] L. Nilsson, O. Groening, O. Kuettel, P. Groening, and L. Schlapbach, "Microscopic characterization of electron field emission," *J. Vac. Sci. Technol. B, Microelectron. Nanometer Struct.*, vol. 20, no. 1, pp. 326–337, Jan./Feb. 2002.

[21] Y. Neo, T. Soda, M. Takeda, M. Nagao, T. Yoshida, C. Yasumuro, S. Kanemaru, T. Sakai, K. Hagiwara, N. Saito, T. Aoki, and H. Mimura, "Focusing characteristics of double-gated field-emitter arrays with a lower height of the focusing electrode," *Appl. Phys. Express*, vol. 1, no. 5, p. 053001, May 2008.

[22] J. Itoh, Y. Tohma, K. Morikawa, S. Kanemaru, and K. Shimizu, "Fabrication of double-gated Si field emitter arrays for focused electron beam generation," *J. Vac. Sci. Technol. B, Microelectron. Nanometer Struct.*, vol. 13, no. 5, pp. 1968–1972, Sep./Oct. 1995.

[23] Y. Yamaoka, S. Kanemaru, and J. Itoh, "Fabrication of silicon field emitter arrays integrated with beam focusing lens," *Jpn. J. Appl. Phys.*, vol. 35, pt. 1, no. 12B, pp. 6626–6628, Dec. 1996.

[24] A. Hosono, S. Kawabuchi, S. Horibata, S. Okuda, H. Harada, and M. Takai, "High emission current double-gated field emitter arrays," *J. Vac. Sci. Technol. B, Microelectron. Nanometer Struct.*, vol. 17, no. 2, pp. 575–579, Mar./Apr. 1999.

[25] Y. Neo, M. Takeda, T. Soda, M. Nagao, T. Yoshida, S. Kanemaru, T. Sakai, K. Hagiwara, N. Saito, T. Aoki, and H. Mimura, "Emission and focusing characteristics of volcano-structured double-gated field emitter arrays," *J. Vac. Sci. Technol. B, Microelectron. Nanometer Struct.*, vol. 27, no. 2, pp. 701–704, Mar./Apr. 2009.

[26] C. A. Bower, K. H. Gilchrist, J. R. Piascik, B. R. Stoner, S. Natarajan, C. B. Parker, S. D. Wolter, and J. T. Glass, "On-chip electron-impact ion source using carbon nanotube field emitters," *Appl. Phys. Lett.*, vol. 90, no. 12, p. 124 102, Mar. 2007.

[27] S. Natarajan, K. H. Gilchrist, J. R. Piascik, C. B. Parker, J. T. Glass, and B. R. Stoner, "Simulation and testing of a lateral, microfabricated electron-impact ion source," *Appl. Phys. Lett.*, vol. 94, no. 4, p. 044 109, Jan. 2009.

[28] R. Baptist, C. Bieth, and C. Py, "Bayard-Alpert vacuum gauge with microtips," *J. Vac. Sci. Technol. B, Microelectron. Nanometer Struct.*, vol. 14, no. 3, pp. 2119–2125, May 1996.

[29] C. Dong and G. R. Myneni, "Carbon nanotube electron source based ionization vacuum gauge," *Appl. Phys. Lett.*, vol. 84, no. 26, pp. 5443–5445, Jun. 2004.

[30] L. Xiao, L. Qian, Y. Wei, L. Liu, and S. Fan, "Conventional triode ionization gauge with carbon nanotube cold electron emitter," *J. Vac. Sci. Technol. A, Vac. Surf. Films*, vol. 26, no. 1, pp. 1–4, Jan. 2008.

[31] W. Knapp, D. Schleussner, and M. Wüest, "Investigation of ionization gauges with carbon nanotube (CNT) field-emitter cathodes," *J. Phys. Conf. Ser.*, vol. 100, p. 092007, 2008.

Liang-Yu Chen received the B.S. degree in electrical engineering and computer science from the University of Hawaii at Manoa, Honolulu, and the M.S. and Ph.D. degrees in electrical engineering and computer science from Massachusetts Institute of Technology (MIT), Cambridge, in 2003 and 2007, respectively. Her Ph.D. research focused on electron-impact ionization, field emission, and field ionization using carbon nanotubes.

She was also with the Microsystems Technology Laboratories, MIT. She is currently working with the Semiconductor Research Development Center, IBM, Hopewell Junction, NY.

Luis Fernando Velásquez-García (M'09–SM'10) received the Mechanical Engineer degree (*magna cum laude* and valedictorian of the School of Engineering) and the Civil Engineer degree (*magna cum laude* and valedictorian of the School of Engineering) from the Universidad de Los Andes, Bogotá, Colombia, in 1998 and 1999, respectively, and the M.S. and Ph.D. degrees from the Department of Aeronautics and Astronautics, Massachusetts Institute of Technology (MIT), Cambridge, in 2001 and 2004, respectively.

In 2004, after completing his studies, he became a Postdoctoral Associate with the Microsystems Technology Laboratories (MTL), MIT, where he was appointed as a Research Scientist in 2005. Since 2009, he has been a Principal Scientist and a Core Member with MTL. He is an expert in micro- and nanofabrication technologies. He has conducted research in micro- and nanotechnologies applied to electrospray, carbon-nanotube-based devices, 3-D packaging, mass spectrometry, nanosatellite propulsion and scientific payload, and chemical reactors. He is the author of more than 18 journal publications and 30 conference-proceeding entries. He is the holder of six patents on microelectromechanical system technologies. His research interests include the application of micro- and nanotechnology to multiplexed scaled-down systems to attain better performance.

Dr. Velásquez-García is a full member of the Sigma Xi Society and a Senior Member of the American Institute of Aeronautics and Astronautics.

Xiazhi Wang, photograph and biography not available at the time of publication.

K. Teo, photograph and biography not available at the time of publication.

Akintunde Ibitayo (Tayo) Akinwande (S'81–M'86–SM'04–F'08) received the B.Sc. degree in electrical and electronic engineering from the University of Ife, Ife, Nigeria, in 1978 and the M.S. and Ph.D. degrees in electrical engineering from Stanford University, Stanford, CA, in 1981 and 1986, respectively.

In 1986, he joined Honeywell International, Inc., Morristown, NJ, where he conducted initially research on GaAs complementary field-effect transistor technology for very high-speed and low-power signal processing. He later joined the Si Microstructures Group, where he conducted research on pressure sensors, accelerometers, and thin-film field emission and display devices. In January 1995, he joined the Microsystems Technology Laboratories, Massachusetts Institute of Technology (MIT), Cambridge, where his research focuses on microfabrication and electronic devices, with particular emphasis on smart sensors and actuators, intelligent displays, large-area electronics (macroelectronics), field-emission and fieldionization devices, mass spectrometry, and electric propulsion. In 2002 and 2003, he was a Visiting Professor with the Department of Engineering and an Overseas Fellow with Churchill College, Cambridge University, Cambridge, U.K., respectively. He is currently a Professor with the Department of Electrical Engineering and Computer Science, MIT. He is the author of more than 100 journal publications. He is the holder of numerous patents in the areas of microelectromechanical systems, electronics on flexible substrates, and display technologies.

Dr. Akinwande is currently a member of the IEEE Nanotechnology Council. He has served on a number of Technical Program Committees for various conferences, including the Device Research Conference, the IEEE International Electron Devices Meeting, the IEEE International Solid-State Circuits Conference, the International Display Research Conference, and the International Vacuum Microelectronics Conference. He was the recipient of the 1996 National Science Foundation CAREER.